The influence of hydrophilicity on the orientational dynamics and structures of imidazolium-based ionic liquid/water binary mixtures

Heather E. Bailey,[a] Yong-Lei Wang,[a] and Michael D. Fayer[b]
Department of Chemistry, Stanford University, Stanford, California 94305, USA

(Received 3 May 2018; accepted 29 June 2018; published online 23 July 2018)

The orientational dynamics and microscopic structures of imidazolium-based ionic liquids of varying hydrophilicity were investigated using optical heterodyne-detected optical Kerr effect (OHD-OKE) spectroscopy and atomistic simulations. Hydrophilicity was tuned via anion selection, cation alkyl chain length, and the addition of a strong hydrogen bond donor on the cation (protic ionic liquid). In the hydrophobic samples, which saturate at relatively low water concentration, OHD-OKE data display Debye Stokes Einstein (DSE) behavior as a function of water concentration. The DSE behavior indicates that the microstructures of the hydrophobic ionic liquid/water mixtures do not fundamentally change as a function of water concentration. The hydrophilic samples have two regimes of different DSE behaviors demonstrating the presence of two structural regimes depending on water concentration. These experimental results indicate that in hydrophilic ionic liquid/water samples, significant structural changes occur to accommodate high water concentrations, while hydrophobic samples become water saturated because the restructuring of local ionic structures is unfavorable. Atomistic simulations show that the local ionic microstructures experience distinct changes in these hydrophilic ionic liquid/water binary samples because of the delicate interplay of intermolecular interactions among imidazolium cations, hydrophilic anions, and water molecules. *Published by AIP Publishing.*
https://doi.org/10.1063/1.5038563

I. INTRODUCTION

Room temperature ionic liquids (RTILs) are a class of charged species that have melting points below room temperature (25 °C). These low melting points are caused by the presence of ions with a combination of asymmetry, large size, and charge delocalization that frustrates crystallization.[1,2] RTILs are widely studied due to their broad range of advantageous properties like low vapor pressure, inflammability, thermal stability, CO_2 solubility, and the presence of extensive nonpolar and polar domains in a neat liquid. These physicochemical properties make RTILs useful candidates for batteries,[3,4] solar cells,[5,6] carbon capture,[7] synthesis,[8] and separations.[9] It is said that there are over one million possible cation and anion combinations that can be used to form RTILs. RTILs have been called designer solvents because they can be optimized for the needs of a particular application by selecting the appropriate combination of constituent ions.

A possible drawback when using RTILs in applications is their hygroscopic nature; water will be present in an application unless expensive measures are taken to dry the RTIL and to prevent it from coming into contact with atmospheric water. In many ionic liquids, the amounts of water picked up from the air will affect macroscopic properties, like viscosity, significantly.[10] The hydrophilicity of ionic liquids varies greatly depending on their structure.[11] Some ionic liquids are relatively hydrophobic and pick up minimal atmospheric water and saturate at low water concentrations, while other ionic liquids pick up water more readily and are infinitely miscible with water.[11] Structural features that affect the hydrophilicity of an RTIL include the cation alkyl chain length,[12] anion,[11,13] and the presence of hydrogen bond donors on the cation [protic ionic liquids (PILs)].[14] The structures of the ionic liquids studied here are given in Fig. 1. Ions at the top of the figure are more hydrophilic.

Changes in macroscopic properties, like viscosity and hydrophilicity, are driven by molecular level structural and dynamical changes. Of particular interest is how hydrophilicity and water miscibility of RTILs are manifested structurally and dynamically. Thus, it is useful to compare structural and dynamical properties of hydrophilic and hydrophobic RTILs at multiple water concentrations. This comparison can help elucidate how RTILs restructure to accommodate increasingly large quantities of water and can provide insight into the driving forces that cause some RTILs to water saturate while others remain infinitely miscible.

Previously, RTIL/water mixtures have been studied using a broad range of methods including optical heterodyne-detected optical Kerr effect (OHD-OKE) spectroscopy,[12,14,15] fluorescence spectroscopy,[16] nuclear magnetic resonance spectroscopy,[17–22] dielectric spectroscopy,[23] and theoretical and computational calculations.[17,24–28] In this paper, we use OHD-OKE spectroscopy in conjunction with atomistic molecular dynamic simulations to better understand the interplay between microstructures and dynamics of RTIL/water

[a]H. E. Bailey and Y.-L. Wang contributed equally to this work.
[b]fayer@stanford.edu. Telephone: 650 723-4446.

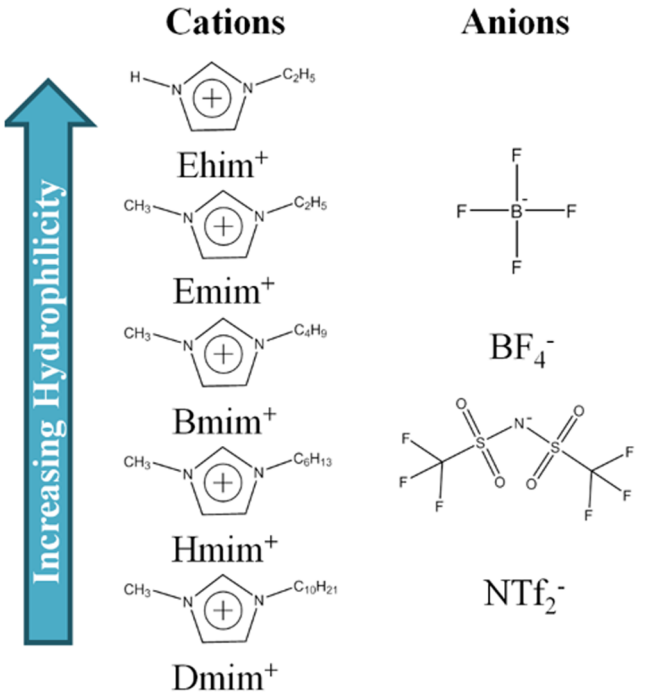

FIG. 1. Chemical structures of the ions composing the ionic liquids studied here. More hydrophilic ions are listed at the top of the figure and the least hydrophilic ions are listed at the bottom. Hydrophilicity was changed by anion selection, cation chain length, and addition of hydrogen bonding groups on imidazolium cations.

binary mixtures. New experimental results are combined with previously published data on RTIL/water mixtures to provide a broader understanding of hydrophilicity in RTILs. The OHD-OKE experiments track the orientational relaxation of RTILs from the picosecond range to complete relaxation many decades later, while atomistic simulations provide corresponding structural information. These methods are used to create a detailed picture of the dynamics and microstructures of RTILs as a function of three methods of tuning hydrophilicity: cation chain length, anion, and presence of strong hydrogen bonding groups in cations.

II. EXPERIMENTAL PROCEDURES

A. Sample preparation and characterization

All RTILs besides 1-ethylimidazolium tetrafluoroborate ($EhimBF_4$) were purchased from Iolitec. The molecular structures of the studied RTILs are given in Fig. 1. Ions at the top of this figure are the most hydrophilic ions. $EhimBF_4$ was synthesized and purified using the methods described by Wu[29] and Burrell.[30] Briefly, 1-ethylimidazole was added in excess to aqueous tetrafluoroboric acid in an ice bath. The mixture was heated to 60 °C for 24 h while stirring. The resulting product was purified through multiple ether washes. The sample was further purified and decolorized using activated charcoal filtration.[31] The product of the synthesis was verified using thermogravimetric analysis and nuclear magnetic resonance spectroscopy, as described in the supplementary material.

All RTILs were dried on a vacuum line at 60 °C for at least 48 h. The water content of all RTILs was measured using Karl Fisher titration (Mettler Toledo). The water content of the dry $EmimBF_4$ and $EhimBF_4$ was 11 ppm and 15 ppm, respectively. The water content of the other RTILs has been reported previously,[12,14,32] but all dry RTILs were well below 100 ppm water. Care was taken to prevent exposure to the atmosphere during data acquisition.

The viscosities of many RTILs as a function of water have been reported previously.[12,14,32,33] The viscosity and liquid density of $EhimBF_4$ RTIL/water mixtures were measured using Cannon-Ubbelohde viscometry and pycnometry, as seen in Table I. Viscosities were measured in a dry box to minimize atmospheric water contaminants. The RTIL/water samples were prepared by mass. All OHD-OKE samples were filtered with a 0.02 μm filter (Whatman Anotop) into 1 cm path length optical grade cuvettes (Starna Cells) and sealed with wax.

B. Optical heterodyne-detected optical Kerr effect spectroscopy

The OHD-OKE experiment is a nonresonant, pump-probe technique that measures the orientational dynamics of bulk liquids.[12,15] The pump pulse creates a slight orientational alignment of the molecules along the pump pulse polarization direction, which results in an induced birefringence. This

TABLE I. Experimental parameters for protic and aprotic ionic liquids.

		NTf_2^-		BF_4^-	
	Ion pair:water	τ (ps)[a]	Viscosity (cP)[a] (24.4 °C)	τ (ps)	Viscosity (cP)[b] (24.4 °C)
	Dry (8550:1)	376 ± 11	36.3	341 ± 5	37.3
	16:1	290 ± 8	28.9	277 ± 11	29.3
	8:1	263 ± 6	26.0	226 ± 8	24.2
	4:1	239 ± 5	21.9	173 ± 8	18.1
	2.6:1	184 ± 6	18.2		
	2:1			128 ± 2	12.3
Emim	1:1			94 ± 4	7.76
	1:2			67 ± 2	4.67
	1:4			46 ± 2	2.88
	1:8			31 ± 1	1.92
	1:16			19 ± 1	1.43
	1:32			18 ± 1	1.19
	1:64			13 ± 1	1.06
	Dry (6500:1)	491 ± 14	57.1	440 ± 11	56.3
	16:1	429 ± 9	50.8	341 ± 17	44.7
	8:1	367 ± 8	44.9	295 ± 14	35.9
	4:1	287 ± 3	32.7	235 ± 6	27.0
	2:1	194 ± 3	24.1	162 ± 9	16.8
	1:1	175 ± 7	15.8	113 ± 6	8.99
Ehim	0.65:1	119 ± 8	11.2		
	1:2			68 ± 3	4.74
	1:4			63 ± 5	2.78
	1:8			44 ± 3	1.99
	1:16			37 ± 3	1.54
	1:32			28 ± 4	1.17
	1:64			19 ± 1	1.15

[a]The values of τ and η for $EmimNTf_2$ and $EhimNTf_2$ were reported by Bailey *et al.*[14]
[b]The viscosity for $EmimBF_4$/water mixtures was reported by Rilo *et al.*[33] The viscosity for $EhimBF_4$/water mixtures is measured here.

alignment (and associated birefringence) decays as the molecules randomize their orientations through equilibrium motions as described by linear response theory.[34] The changes in induced birefringence are measured with heterodyne detection when the combined signal and local oscillator (LO) pass through a polarizer that nulls the probe but not the signal/LO.

The OHD-OKE experimental setup has been described in detail previously.[12,15] The key components are presented below. The ultrafast pulses necessary for the experiment are generated by a Ti:sapphire oscillator/5 kHz Ti:sapphire regenerative amplifier. These amplified pulses are beam split into a strong pump beam and a weak probe beam. The pump pulses arrive at the sample linearly polarized, while the probe pulses are polarized at ±45° relative to the pump. The time dependence is measured through the variable mechanical delay of the probe pulses using a delay line. Heterodyne detection is implemented through the slight depolarization of the probe pulse. This creates the collinear LO that couples with the signal and enables phase cycling, which greatly improves the signal to noise ratio.[34,35] OHD-OKE is a particularly useful method due to its ability to track dynamics over an exceptionally long time range (picoseconds to the end of the orientational dynamics up to tens of microseconds). Additionally, the nonresonant nature of the experiment means that any molecule with anisotropic polarizability contributes the signal and a probe impurity does not need to be added. It is also a spectroscopic technique that is measured entirely in the ground state, so it is minimally perturbative. OHD-OKE can directly study the molecule of interest in its ground state.

While OHD-OKE measures unique and useful dynamical information, extracting meaningful, quantitative information can be difficult. After very short time, when molecular collisions create multi-particle distortions that contribute to the signal, OHD-OKE measures the time derivative of the polarizability-polarizability correlation function (orientational correlation function). This correlation function can be found by coupling it to the density correlation function using schematic mode coupling theory (MCT).[36] Solving the MCT equations requires significant computational resources, and the exact solutions are very complicated. The general functional form of the correlation function is multiple power law decays followed by a final exponential.[37] The power laws describe a series of local caging motions that occur at short time. A final exponential decay reports on the final complete randomization of the molecular orientations. This exponential can be related to physical properties, e.g., the viscosity, to gain an understanding of the dynamics.

It is important to note that all of these orientational relaxation processes are not simultaneously occurring. The power law caging motions are limited to early time, and the long-time exponential behavior occurs only after the caging motions are nearly complete. Thus, to fit the data, the long-time data can be fit simply as a single exponential. This is done repeatedly over multiple time ranges to ensure that the power law dynamics are not bleeding into the fit. This can be repeated with power laws for the caging region of the dynamics. To fit the complete decay while accounting for overlap in time of the different randomization processes, a phenomenological fitting function, which reproduces the functional form obtained from MCT, is given in the following equation:

$$F(t) = \frac{B}{2}\left(1 - erf\left(\frac{(\ln(t) - n)}{\sqrt{2}u}\right)\right)t^{-b} + \frac{C}{2}\left(1 + erf\left(\frac{\ln(t) - n}{\sqrt{2}u}\right)\right)e^{-t/\tau} + y_0. \quad (1)$$

This fitting function has been described thoroughly previously.[14] The first term describes the von Schweidler power law with exponent b. Additional power law terms can be added as necessary. The final term describes the final exponential with time constant, τ. Due to the large number of variables in Eq. (1), the values of b and τ from the initial fits of each process are used.

C. Atomistic molecular dynamic simulations

Atomistic interactions for the $Emim^+$ and $Ehim^+$ cations and the BF_4^- anions were taken from a systematically developed force field in previous studies based on the AMBER framework.[14] The SPC/E water model (extended simple point charge model) with constrained covalent bonds was employed in the current work. The cross-interaction parameters between different atom types were obtained from the Lorentz-Berthelot combination rules. The detailed simulation system compositions of the $EmimBF_4$ and $EhimBF_4$ RTIL/water mixtures were determined to match the experimental RTIL/water binary mixture compositions as listed in Table I.

Atomistic molecular dynamic simulations were performed using the GROMACS 5.0.4 package with cubic periodic boundary conditions.[38] The equations of motion were integrated using a classic Verlet leapfrog integration algorithm with a time step of 1.0 fs. A cutoff radius of 1.6 nm was set for short-range van der Waals interactions and real-space electrostatic interactions. The particle-mesh Ewald summation method with an interpolation order of 5 and Fourier grid spacing of 0.12 nm was employed to handle long-range electrostatic interactions in the reciprocal space. All simulation systems were first energetically minimized using a steepest descent algorithm and thereafter annealed gradually from 800 to 300 K within 10 ns. The annealed simulation boxes were equilibrated in an isothermal-isobaric ensemble for 40 ns and maintained using a Nosé-Hoover chain thermostat and a Parrinello-Rahman barostat with time coupling constants of 500 and 200 fs, respectively, to control temperature at 300 K and pressure at 1 atm. Canonical ensemble simulations were further performed for 50 ns for all RTIL/water mixtures, and simulation trajectories were recorded at an interval of 100 fs for further microstructural and dynamical analyses.

III. RESULTS AND DISCUSSION

A. Source of OHD-OKE signal

The RTILs studied in this work include dry RTILs (<100 ppm water) and RTIL/water mixtures with varied water concentrations. To effectively interpret the OHD-OKE data and make meaningful comparisons between the different RTIL samples, it is important to consider the source of the signal. The

RTIL samples studied in this work consist of cations, anions, and water molecules that could be overlapping sources of signal. The OHD-OKE experiments measure the time derivative of the polarizability-polarizability correlation function. After short time scale molecular interactions that influence the samples' polarizability, this correlation function is dominated by or totally arises from the orientational correlation functions of the molecules that make up the sample.[39,40] Any species with anisotropic polarizability contributes to the signal.

Water has a very small anisotropic polarizability relative to RTILs. Previous experiments that compared the signal strength of water and imidazolium based RTILs showed that water produced a negligible contribution to the signal.[41–43] Thus, we can assume that water molecules do not contribute significantly to any of the RTIL samples measured below. Next, considering the anions, it is clear that BF_4^- does not have significant single particle anisotropic polarizability due to its tetrahedral geometry and high degree of symmetry. This is less obvious for NTf_2^- anion due to its asymmetry and large size. Calculations concerning the effects of anionic and cationic substitutions on the ultrafast solvent dynamics of imidazolium-based RTILs and NTf_2^-based RTILs have shown that NTf_2^- anions contribute negligibly to the anisotropic polarizability of the entire ionic liquids.[44]

This suggests that the OHD-OKE signal in these RTIL/water mixtures mainly originates from the imidazolium cations. The final consideration is whether this anisotropic polarizability can be attributed predominantly to one part of the cation. This is particularly important in the comparison between RTILs with different alkyl groups on the cation. Previous comparisons of OHD-OKE data for imidazolium-based RTILs and long-chained alkanes showed that the imidazolium head groups contributed at least four times more signal than alkanes.[15] Based on these considerations, in all the samples studied here, the OHD-OKE signal originates primarily from the imidazolium head groups. However, the OHD-OKE data provides information on total solvent orientational and structural randomization because the imidazolium head group moiety cannot reorient without the reorientation of all species that compose the liquid. In liquids with these large cations and anions, orientational relaxation of the cation head group will not occur without considerable structural randomization of the entire liquid.

B. Comparison of dry BF_4^- and NTf_2^- ionic liquids

The anion is one of the strongest influences on the miscibility of an RTIL with water.[13,27] Two common anions, BF_4^- and NTf_2^-, are characterized by very hydrophilic and hydrophobic features, respectively. The difference in physicochemical properties between RTILs with these two anions is evident even in the dry RTIL samples. The viscosities of a series of imidazolium-based cations paired with each anion are given in Table II. When there is no extended nonpolar region in the RTIL matrices (i.e., $Emim^+$), the liquid viscosities of the two RTILs are approximately the same (36.3 cP *vs.* 37.3 cP). However, the difference in viscosity increases with longer aliphatic chains in imidazolium cations. The liquid viscosity of $DmimBF_4$ is 4.4 times larger than that of $DmimNTf_2$.

TABLE II. Key experimental parameters for dry NTf_2^- and BF_4^- based ionic liquids.

	BF_4^-		NTf_2^-	
Cation	η (cP)	τ (ps)	η (cP)	τ (ps)
$Emim^+$	37.3[a]	341 ± 5	36.3[b]	376 ± 11[b]
$Bmim^+$	103[c]	1400 ± 140[c]	59.3[d]	1160 ± 30[d]
$Hmim^+$	190[c]	3950 ± 395[c]	82.3[d]	2080 ± 50[d]
$Dmim^+$	630[c]	9980 ± 998[c]	143.6[d]	4630 ± 200[d]

[a]Value reported by Rilo *et al.*[33]
[b]Value reported by Bailey *et al.*[14]
[c]Value reported by Sturlaugson *et al.*[12]
[d]Value reported by Thomaz *et al.*[63]

To compare the orientational dynamics of the RTILs with different anions, OHD-OKE experiments were conducted on dry $EmimBF_4$, $BmimBF_4$,[12,45] $HmimBF_4$,[12] and $DmimBF_4$[12] and the equivalent NTf_2^- RTILs.[16] Some individual results have been published before, but they have not been analyzed in combination with access trends.

The OHD-OKE data were fit using Eq. (1) to extract the value of τ. For hydrodynamic liquids, the relationship between viscosity and τ can be described by the Debye Stokes Einstein (DSE) equation, as given in the following equation:

$$\tau_{self} = \frac{\eta(T)Vf_\theta C}{k_B T}, \tag{2}$$

where τ_{self} is the single molecule rotational self-diffusion time for a symmetric top, η is the shear viscosity, V is the volume of the rotator, k_B is the Boltzmann constant, T is the absolute temperature, f_θ is a shape factor that accounts for friction due to the deviation of the rotator from sphericity, and C is an interaction factor that accounts for friction due to the rotator interacting with neighboring species. In general, OHD-OKE measures collective reorientation instead of single molecule reorientation, so additional terms are needed to relate τ from Eq. (1) to τ_{self} from Eq. (2). This relationship is given by the following equation:

$$\tau = \frac{g_2}{j_2}\tau_{self}, \tag{3}$$

where g_2 is the static orientational correlation function and j_2 is the dynamic orientational correlation function. j_2 has been calculated as 1 for a wide range of liquids.[46–48] If there are long lived structural correlations that remain for times long compared to the single molecule orientational relaxation and have associated with these correlations a residual anisotropic polarizability induced by the pump pulse, then τ can be somewhat longer than τ_{self}. Here we assume that τ is equal to τ_{self}, i.e., j_2 is indeed 1. g_2 describes time-independent orientational correlation which deviates from unity in non-isotropic liquids where multiparticle pair correlations influence the relaxation of the induced polarizability anisotropy. Equations (2) and (3) are combined for use with OHD-OKE data.

To test a liquid for hydrodynamic behavior, τ can be plotted against viscosity. The DSE plots for dry BF_4^- and dry NTf_2^- imidazolium-based RTILs with varied aliphatic chains are shown in Fig. 2. These dry RTILs exhibit hydrodynamic

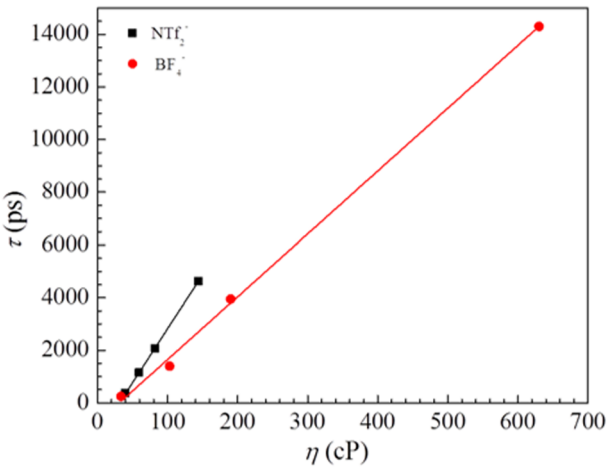

FIG. 2. The Debye Stokes Einstein plots for dry 1-alkyl-3-methylimidazolium tetrafluoroborates (red) and 1-alkyl-3-methylimidazolium bis(trifluoromethylsulfonyl)imide (black). Both sets of data are linear, indicating DSE behavior.

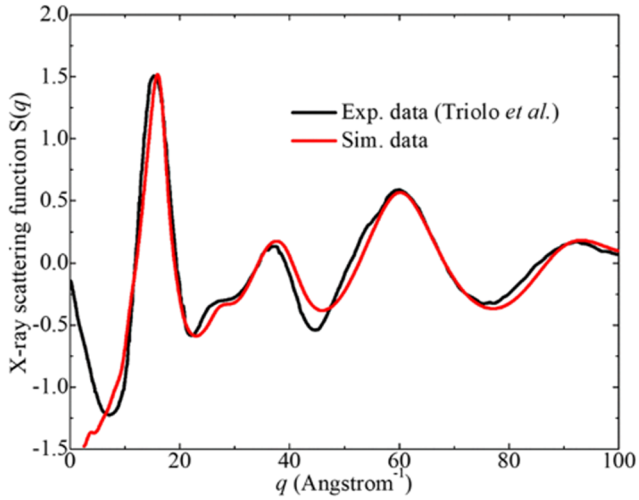

FIG. 3. Comparison of computational X-ray scattering static structural factor $S(q)$ for dry $EmimBF_4$ with experimental data in the range of $q \leq 100.0$ Å^{-1}. The experimental data were obtained from the literature.[49]

behavior as evidenced by the linearity of both sets of experimental data. However, the slopes of the two lines are very different, and this can provide insight into the differences between the two types of ionic liquids.

Based on the combination of Eqs. (2) and (3), five variables comprise the slope. As described above, OHD-OKE signal primarily comes from the imidazolium head groups in these dry RTIL samples. Since the same imidazolium cations are being compared, the static orientational correlation function, the volume, and the shape factor must remain constant between the sets of RTIL samples. All experiments were conducted at the same experimental temperature. The only variable that can cause this slope change is C, the interaction factor. The RTIL samples containing NTf_2^- anions have a higher slope, indicating that imidazolium cations in these RTILs experience stronger intermolecular interactions than their counterparts in RTIL samples containing BF_4^- anions.

To better understand the microstructures of the systems that underlie the different DSE slopes, atomistic simulations were conducted. The force fields used in the atomistic simulations can be validated by comparing the available experimental value of the X-ray scattering structure factor, $S(q)$, for the dry $EmimBF_4$ RTIL to the curve calculated with the simulations. It is shown in Fig. 3 that the computated $S(q)$ matches the experimental X-ray scattering functions for the dry $EmimBF_4$ RTIL very well.[49] This demonstrates that the force field parameters for the RTILs in the current work are accurate enough to describe thermodynamics and microstructures of these RTILs and RTIL/water mixtures. X-ray data are not available for the water mixtures. Therefore, furthermore, the experimental and simulated liquid densities were compared; they matched within the experimental error at all water concentrations. This further validates the force fields used at different hydration levels.

Figure 4 presents the radial distribution functions (RDFs) of the cation-cation (a), anion-anion (b), and cation-anion (c) pairs in the dry $EmimBF_4$ and $EmimNTf_2$ RTIL samples, as calculated using the force fields validated above. The center-of-mass of the imidazolium ring planes in the $Emim^+$ cations, the B atoms in the BF_4^- anions, and the N atoms in the NTf_2^- anions are taken as reference sites to calculate these intermolecular RDFs. The cation-cation RDFs [panel (a)] show that the $Emim^+$ cations are experiencing different

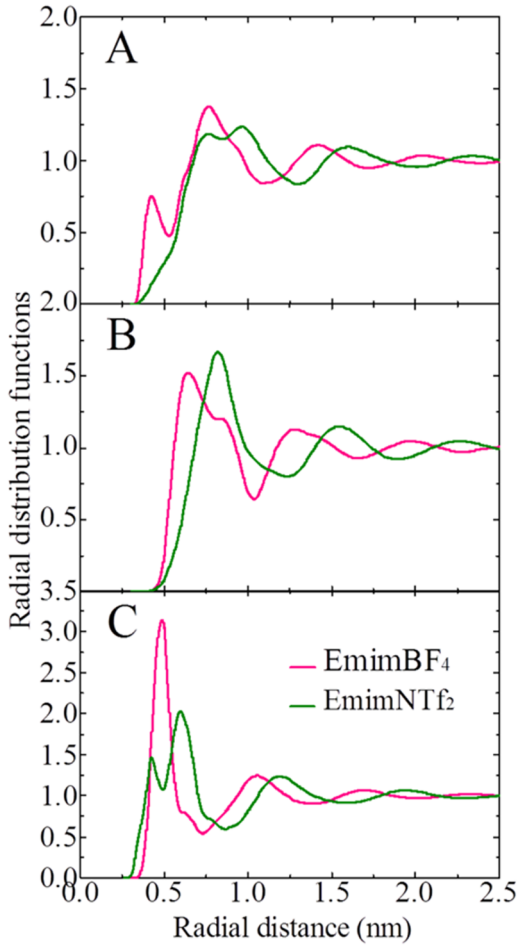

FIG. 4. Radial Distribution Functions of (a) cation-cation, (b) anion-anion, and (c) cation-anion pairs for dry $EmimBF_4$ and $EmimNTf_2$.

microstructural environments in these two dry RTIL samples. The prepeak registered at 0.42 nm indicates the formation of preferential π-π stacking motifs between imidazolium ring planes in the $EmimBF_4$ RTIL sample, whereas in $EmimNTf_2$, there is no such prepeak, indicating that there are almost no π type stacking interactions between the imidazolium ring planes in the $Emim^+$ cations.[50–54] The large NTf_2^- anions either take preferential on-top distributions above and below the imidazolium ring planes or exhibit tilted coordinations with imidazolium ring planes in their equatorial region, leading to π type stacking associations between neighboring imidazolium ring planes being screened due to anionic size effects. Additionally, the NTf_2^- anions have multiple hydrogen bonding acceptors, such as one N atom and four O atoms that are covalently bonded to the S atoms in the anionic framework. These hydrogen bonding acceptors prefer to coordinate with the hydrogen atoms in the imidazolium rings in the $Emim^+$ cations, leading to the formation of multiple hydrogen bonds or a hydrogen bond network within the RTIL matrices.[14,17,21,53] It should be noted that the hydrogen atoms in the imidazolium rings do not coordinate with the F atoms in the NTf_2^- anions via hydrogen bonding interactions due to their lower electronegativities in the anionic framework. However, these hydrogen atoms tend to form hydrogen bonds with the F atoms in the BF_4^- anions but with decreased hydrogen bond directionality and strength.

The bifurcated feature in the cation-cation [panel (a)] and cation-anion [panel (c)] RDF plots in the $EmimNTf_2$ RTIL sample corresponds to the existence of *cis* and *trans* conformations for NTf_2^- anions in the RTIL, as we have discussed in a prior work.[14] Both the *cis* and *trans* conformations of the NTf_2^- anions in imidazolium-based RTIL samples contribute to significant intermolecular interactions between imidazolium cations and NTf_2^- anions via strong Coulombic interactions among polar moieties and preferential van der Waals interactions among nonpolar groups, as well as other delicate interactions like hydrogen bonding and π stacking interactions. Additionally, NTf_2^- anions can mediate the relative distributions of the imidazolium ring planes in the dry RTIL matrices and RTIL/water mixtures as discussed in previous publications due to the existence of multiple hydrogen bonding acceptors in the anionic framework.[14,17,21,53]

The first peak in the anion-anion RDFs [panel (b)] of $EmimBF_4$ is observed at a shorter radial distance due to the smaller anionic sizes of BF_4^- relative to NTf_2^- anions. The BF_4^- anions mainly occupy equatorial positions in the imidazolium ring planes, on the one side, promoting the intermolecular hydrogen bonding interactions between close contacted ion pairs and, on the other side, stabilizing the striking π-π stacking structures between neighboring imidazolium ring planes. The NTf_2^- anions have a larger anionic size than the BF_4^- anions and are characterized by multiple strong hydrogen bonding interactions with imidazolium cations, all of which lead to their stronger coordination with imidazolium cations in RTIL samples, as manifested in liquid densities of these two dry RTIL samples. As such, the slope of the DSE plot for the NTf_2^- based RTILs is much larger than that for BF_4^- analogs, as shown in Fig. 2.

C. Comparison of wet BF_4^- and NTf_2^- ionic liquids

This leads to the question of how anion selection influences hydrophilicity and water miscibility. To look at how the anion affects these properties, $EmimBF_4$ was compared to $EmimNTf_2$ at various water concentrations. $EmimBF_4$ is infinitely miscible with water, while $EmimNTf_2$ is relatively hydrophobic and saturates with water at 2.6 ion pairs per water. The OHD-OKE data for $EmimBF_4$ RTIL/water mixtures are displayed in Fig. 5(a). Note that the logarithmic axes and the decays have been vertically offset for clarity. The OHD-OKE decays for $EmimNTf_2$ RTIL/water mixtures have been reported previously.[14]

Figure 6 gives the DSE plots for $EmimNTf_2$/water mixtures (black) and for $EmimBF_4$/water mixtures (blue). The $EmimNTf_2$ DSE plot is linear through the saturation point, while the $EmimBF_4$ DSE plot shows two distinct linear regions. The slope of the DSE plot for $EmimNTf_2$ RTIL/water mixtures with varied water concentrations is slightly larger than that for $EmimBF_4$ RTIL/water mixtures with comparable water concentrations, which is attributed to stronger intermolecular interactions among $Emim^+$ cations, NTf_2^- anions, and water molecules as compared to their counterparts in $EmimBF_4$ RTIL/water mixtures, as has been discussed in

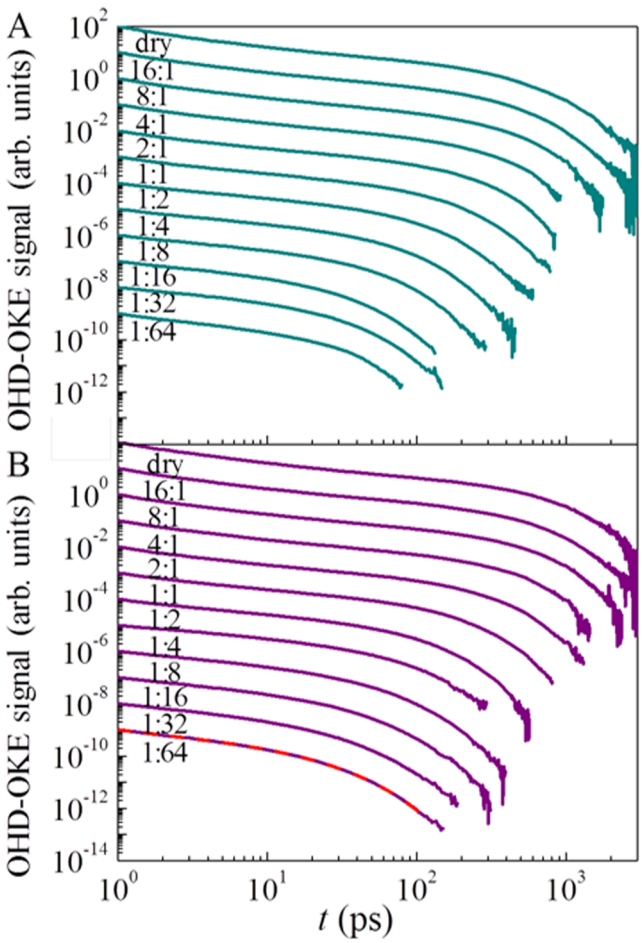

FIG. 5. OHD-OKE data for (a) $EmimBF_4$ and (b) $EhimBF_4$ at twelve water concentrations ranging from dry to 1:64 ion pairs:water. The data are plotted on logarithmic axes and vertically offset for clarity. A sample fit using Eq. (1) is shown on the 1:64 data in panel (b). All fits were of similar quality.

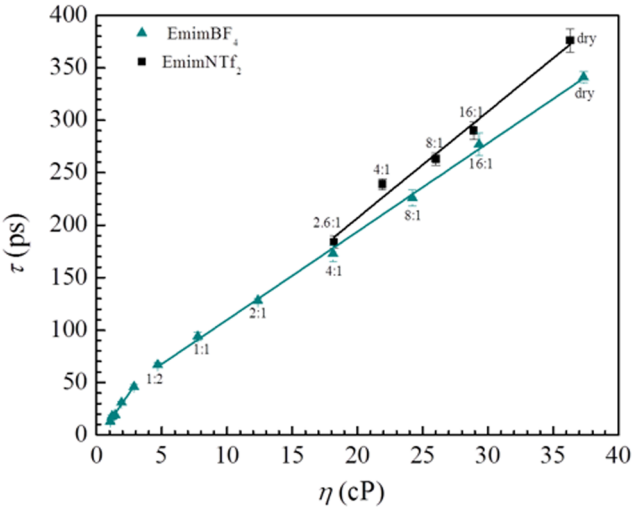

FIG. 6. The Debye Stokes Einstein plot for $EmimBF_4$/water mixtures (blue) and $EmimNTf_2$/water mixtures (black). $EmimNTf_2$ has one linear regime while $EmimBF_4$ has two linear regimes.

Subsection III B. Additionally, this observation can provide further insight into how hydrophilicity influences microstructures and dynamics of ionic species in RTIL/water mixtures. In the case of $EmimBF_4$, the first linear region ends around 1:2 ion pairs:water and the next linear region starts at 1:4 ion pairs:water, although there may be a crossover region. These results suggest that there is no significant microstructural change that occurs with the gradual addition of water molecules to $EmimBF_4$ RTIL/water mixtures up to the 1:2 ion pairs:water concentration. The $Emim^+$ cations and BF_4^- anions slightly adjust their relative positions in the local ionic environment to accommodate more water molecules, which is corroborated through the visualization of the simulation trajectories of the corresponding atomistic simulation systems and the calculation of intermolecular RDFs between the $Emim^+$ cations and the BF_4^- anions, which will be discussed in Subsection III D.

The dual nature of water molecules in hydrogen bonding interactions enables water molecules to act as both hydrogen bond donors to BF_4^- anions with F atoms as hydrogen bonding acceptors and as hydrogen bond acceptors for hydrogen atoms in imidazolium rings in $Emim^+$ cations. These interactions contribute to water's segregated distribution between imidazolium rings and BF_4^- anions, and the local ionic structures are characterized by solute-shared ion pairs through the formation of cation-water-anion triple complexes.[26,28] However, when more water molecules are introduced into $EmimBF_4$/water mixtures, the ions must reorient considerably to accommodate more water molecules. This microstructural change is reflected by the new linear regime at a high water content in the DSE plot. If it were unfavorable to reorganize the local ionic structures in RTIL/water matrices, the RTIL would saturate at ~1:2 ion pairs:water. This behavior is observed in $EmimNTf_2$ which is linear through the saturation point at 2.6:1 ion pairs:water. It is unfavorable to change the extended structure of the ionic liquid. As discussed in Subsection III B, the NTf_2^- anions have stronger interactions with the $Emim^+$ cations through decisive Coulombic interactions and preferential hydrogen bonding coordinations. The implication is that it is unfavorable to break these interactions to allow more water into the constructed and stable ionic environments in $EmimNTf_2$, so the $EmimNTf_2$ RTIL quickly saturates.

D. Comparison of protic and aprotic ionic liquids

Another method of tuning hydrophilicity is by adding a strong hydrogen bond donor to the cation, creating a protic ionic liquid. Previously, OHD-OKE spectroscopy and atomistic simulations were used to compare $EmimNTf_2$ and its protic analog $EhimNTf_2$.[14] These two RTILs water saturate at 2.6:1 ion pairs:water and 0.65 ion pairs:water, respectively. The DSE plot of the $EmimNTf_2$ RTIL/water mixtures was linear, while the DSE plot of $EhimNTf_2$ was linear through the 2:1 sample. At higher water concentrations, there was a discontinuity in the DSE plot indicating that the rotator (cation) was experiencing higher friction. Atomistic simulations and linear infrared spectroscopy (FT-IR) attributed this deviation from hydrodynamic behavior to the formation of water clusters (pairs) coupling the cation and anion. It should be noted that this deviation was beyond the water saturation point of $EmimNTf_2$. This deviation is different from the two linear DSE regimes that were observed in $EmimBF_4$ RTIL/water mixtures, as shown in Fig. 6, as the slope is the same before and after the discontinuity.

To elucidate the microstructures and dynamics of a hydrophilic aprotic RTIL that is infinitely miscible with water and its protic analog, $EmimBF_4$ and $EhimBF_4$ were studied at 12 water concentrations ranging from dry to 1:64 ion pairs:water. The OHD-OKE decays are shown in Fig. 5. Note that the logarithmic axes and the decays are offset for clarity. The experimental OHD-OKE decays for $EmimBF_4$ and $EhimBF_4$ RTIL/water mixtures are shown in panels (a) and (b), respectively. A sample fit using Eq. (1) is shown with a red dashed line on the 1:64 $EhimBF_4$ data. All fits were of similar quality. Additional fits are shown in the supplementary material.

The most interesting component of these fits is the long time exponential region, which in all samples is single exponential, quantified by τ from Eq. (1). Previously, biexponential behavior has been observed in imidazolium-based BF_4^- RTILs but only for imidazolium cations with long alkyl chains as gel formation is approached.[12] Since the longest alkyl chain length in these RTIL/water samples is an ethyl chain, it is consistent with prior measurements that the data presented in Fig. 5 exhibit single exponential behavior. The time constant, τ, associated with the single exponential [Eq. (1)] can be related to viscosity, η, by combining Eqs. (2) and (3). The values of τ and η are given in Table I.

The DSE plots for the $EmimBF_4$ and $EhimBF_4$ RTIL/water mixtures are shown in Fig. 7. For both sets of RTIL/water mixtures, it appears that there are two hydrodynamic regimes with a crossover region in between. For samples drier than 1:2 ion pairs:water, the plot is linear, which suggests that the microstructures in these RTIL/water mixtures do not have to fundamentally change in order to accommodate the increasing amount of water. This changes at around 1:4 ion pairs:water, where the DSE plot enters a new linear regime,

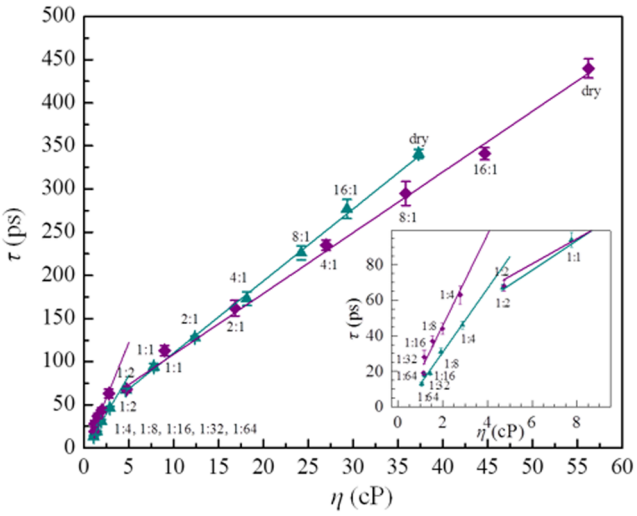

FIG. 7. The Debye Stokes Einstein plot for $EmimBF_4$/water mixtures (blue) and $EhimBF_4$/water mixtures (purple). Both data sets are linear through the 1:2 sample. A new Debye Stokes Einstein regime is entered at higher water concentrations, as shown in the inset. Lines are included as guide to the eye.

with a steeper slope, as shown in the inset of Fig. 7. This indicates that this is the critical concentration where these two RTILs would saturate if it was not favorable to restructure. This observation is in contrast to what was seen in the $EmimNTf_2$ RTIL/water mixtures, which had a linear DSE plot up to its saturation concentration.[14]

Some structural information can be obtained by looking at the liquid densities of these four RTIL/water mixtures as a function of water content; the experimental and computational densities are plotted in Fig. 8 as solid and outlined data points, respectively. The experimental liquid densities for

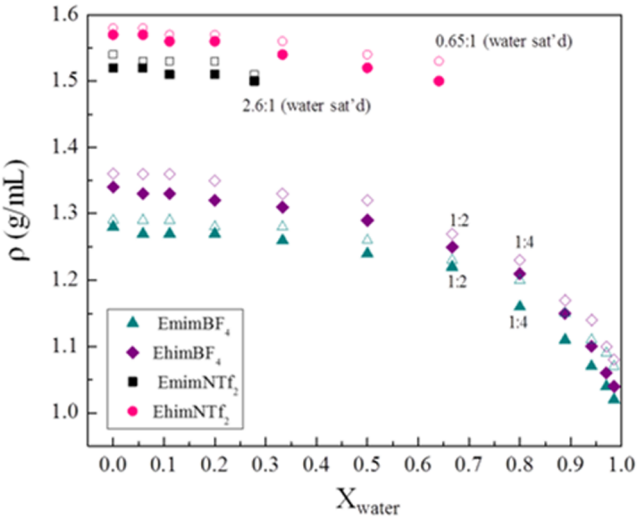

FIG. 8. Experimental and computational liquid densities of $EmimNTf_2$ (black), $EhimNTf_2$ (pink), $EmimBF_4$ (blue), and $EhimBF_4$ (purple) as a function of water concentration. The experimental densities of $EmimBF_4$ (solid symbols) were interpolated from the literature.[55] The computational density data (outlined symbols) for NTf_2-based RTIL/water mixtures are taken from a previous work,[14] and the computational density results for BF_4^--based RTIL/water mixtures are obtained from atomistic simulations in the current work.

$EmimBF_4$ RTIL/water mixtures were obtained from the literature.[55] All other experimental densities were measured via pycnometry. The computational liquid densities of these four RTIL/water mixtures are obtained from the current isothermal-isobaric atomistic simulations. For the hydrophobic NTf_2-based RTIL/water mixtures, the liquid density decreases by 1.3% for $EmimNTf_2$ and 4.7% for $EhimNTf_2$, respectively, before these two RTILs become water saturated. For the hydrophilic, infinitely miscible BF_4-based RTIL/water mixtures, the liquid density changes more significantly. Through the 1:2 sample (the last of the first hydrodynamic regime in the DSE plots), the liquid density has decreased by 4.9% in $EmimBF_4$ and by 7.2% in $EhimBF_4$. After this concentration, the liquid density begins to drop very quickly as it approaches the density of neat water. These changes are corroborated by computational liquid densities of these RTIL/water mixtures. The change in the slope in the liquid density data with increasing water content and the onset of speed up of the dynamics at the same water concentrations supports the proposition that these RTIL/water systems undergo fundamental structural changes at these specific concentrations. It should be noted that the water dependence of the liquid density of typical molecular liquids often decrease linearly at all water concentrations.[56] This is in contrast to the observations in these RTIL/water mixtures where liquid density remained nearly constant over a wide range of water concentrations.

In addition to liquid densities, atomistic simulations give additional physical insight into the microscopic ionic structures of these RTIL samples and microstructural changes that occur in the four RTIL/water mixtures with increasing water concentrations. The cation-cation and anion-anion RDFs for these four RTIL/water mixtures with varied water concentrations are calculated with the atomistic simulations and are shown in Figs. 9 and 10. In NTf_2-based RTIL/water mixtures, the progressive addition of water leads to negligible changes in the cation-cation coordination structures, as shown by the prominent bifurcated characteristics seen in the cation-cation RDF plots in Fig. 9. A rationale for this computational observation is that the introduced water molecules are mainly dispersed in cavities between the imidazolium cations and the NTf_2^- anions because of the existence of multiple hydrogen bonding donors in imidazolium cations and multiple hydrogen bonding acceptors in NTf_2^- anions, as has been extensively discussed in a prior work.[14] However, in BF_4^- based RTIL/water mixtures, the gradual addition of water molecules results in distinct changes among the imidazolium ring planes in the cations. As shown in Fig. 4, the prepeaks in the cation-cation RDF plots of the BF_4^- based RTILs correspond to the formation of π-π stacking structures between imidazolium ring planes in the $Emim^+$ cations. The gradual addition of water molecules to the RTIL matrices leads to the decreased amplitude of these prepeaks in both the $EmimBF_4$ and $EhimBF_4$ RTIL/water mixtures. This observation indicates a weakening of intermolecular interactions between the imidazolium ring planes in the $Emim^+$ and $Ehim^+$ cations due to the dispersed distribution of water molecules between the imidazolium cations and the BF_4^- anions. Additionally, the magnitude of the π-π stacking coordination between

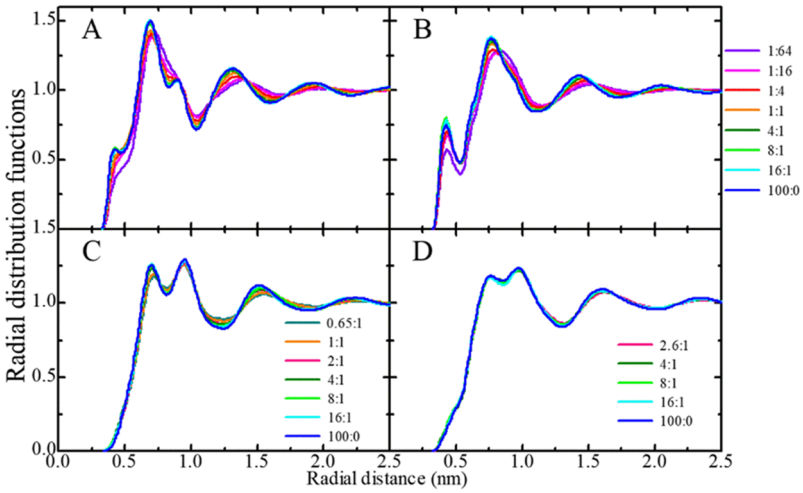

FIG. 9. Cation-cation RDFs in RTIL/water mixtures with varied RTIL:water ratios. (a) $EhimBF_4$, (b) $EmimBF_4$, (c) $EhimNTf_2$, and (d) $EmimNTf_2$.

imidazolium ring planes in the $EmimBF_4$ RTIL/water mixtures is much stronger than that in the $EhimBF_4$ RTIL/water mixtures. This can be understood by the competitive feature of hydrogen bonding interactions and π-π stacking associations between imidazolium ring planes and anionic groups.[50,54,57] The preferential hydrogen bonding interactions among $Ehim^+$ cations, BF_4^- anions, and water molecules compete more favorably with the π-π stacking associations between $Ehim^+$ cations in determining local ionic structures in $EhimBF_4$ RTIL/water mixtures.

For the cation-anion RDFs (shown in the supplementary material) in all the RTIL/water mixtures studied here and the anion-anion RDFs (shown in Fig. 10) in the NTf_2^- based RTIL/water mixtures, there are no obvious changes in microstructures in the local ionic environments. The negligible changes in the cation-anion RDFs in all of the RTIL/water mixtures can be attributed to attractive Coulombic interactions between imidazolium cations and anionic groups. No matter how hydrogen bonding interactions between imidazolium cations and anionic groups compete with π-π stacking coordinations between imidazolium ring planes in RTIL/water mixtures, the attractive Coulombic interactions between the imidazolium cations and anionic groups are far stronger than any other intra- and inter-molecular interactions in dominating the striking cation-anion coordination structures in RTIL/water mixtures.

In the anion-anion RDFs in NTf_2^- based RTIL/water mixtures, as shown in Fig. 10, the introduced water molecules tend to disperse in cavities between imidazolium cations and NTf_2^- anions due to the dual nature of water molecules in hydrogen bonding with both imidazolium cations and NTf_2^- anions. The existence of multiple hydrogen bonding donors in the imidazolium cations and multiple hydrogen bonding acceptors in the NTf_2^- anions indicate that NTf_2^- based RTIL matrices can accommodate a non-negligible number of water molecules before saturation.[14,17,18,20,21] The dispersed water molecules, or even the accumulated small water clusters between neighboring imidazolium cations and NTf_2^- anions, have difficulty disturbing the prominent cation-anion microstructures in NTf_2^- based RTIL/water mixtures. However, in BF_4^- based RTIL/water mixtures, a gradual addition of water molecules into the RTIL matrices tends to mediate the relative distribution of BF_4^- anions. In the anion-anion RDF plots for BF_4^-based RTIL/water mixtures, the first peaks are registered at around 0.61 nm and the second peaks are located at approximately 0.84 nm, respectively. Such a double-peak plot indicates a

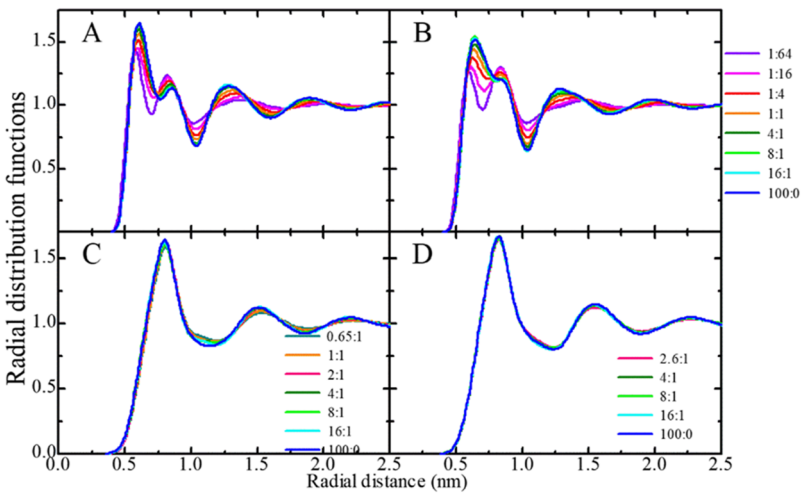

FIG. 10. Anion-anion RDFs in RTIL/water mixtures with varied RTIL:water ratios. (a) $EhimBF_4$, (b) $EmimBF_4$, (c) $EhimNTf_2$, and (d) $EmimNTf_2$.

multiple coordination pattern of BF_4^- anions around the imidazolium ring planes because there are multiple hydrogen bonding donors in imidazolium cations.

A gradual addition of water molecules into BF_4^- based RTIL/water mixtures weakens the first anion-anion coordination pattern and strengthens the second association feature due to the dispersed distribution of water molecules between imidazolium cations and BF_4^- anions. The representative liquid morphologies of $EmimBF_4$ RTIL/water mixtures with varied water concentrations are shown in Fig. 11. In these BF_4^- based RTIL/water mixtures with a small water concentration, the spatial distribution of water molecules between imidazolium cations and BF_4^- anions and the formation of cation-water-anion triple complexes in the RTIL/water mixtures [Fig. 11(b)] are similar to that observed in NTf_2^- based RTIL/water mixtures with comparable water concentrations. However, as more water molecules are introduced into BF_4^- based RTIL/water mixtures, these water molecules tend to form water clusters [Fig. 11(c)], water chain-like structures [Fig. 11(d)], water channels connecting multiple anions [Fig. 11(e)], and finally leads to the formation of a water network [Fig. 11(f)] throughout the entire simulation box. These water aggregates are capable of breaking the hydrogen bonds formed between the fluorine atoms in the BF_4^- anions and the hydrogen atoms in the imidazolium cations and thus weakens the first anion-anion coordination pattern, as shown in Fig. 10. Such striking changes in the microscopic ionic structures in the RTIL/water mixtures are qualitatively manifested in the corresponding spatial coordinations of constituent ions with water molecules, as shown in representative cation-water, anion-water, and water-water RDFs in the supplementary material.

The distinct microstructures in the dry RTIL samples and the striking microstructural changes in the corresponding RTIL/water mixtures as water concentration increases are also reflected in dynamical quantities of the imidazolium cations. In the current work, the reorientational dynamics of the imidazolium ring planes are represented by the second-rank Legendre polynomial correlation function, $P_2(t) = \langle \bar{e}(0)\bar{e}(t)\rangle$, of the normal vector $\bar{e}$ to the center-of-mass of imidazolium ring planes.[53,54,57] Representative reorientational correlation functions of the imidazolium ring planes for all of the RTIL/water mixtures with varied water concentrations are presented in the supplementary material. In a given RTIL matrix, the decay of the reorientational correlation functions for imidazolium ring planes becomes faster as water concentration increases in RTIL/water mixtures, as seen in the OHD-OKE data. This is attributed to the fact that the introduced water molecules, either in small water clusters or in large water aggregates, tend to weaken the attractive Coulombic interactions between imidazolium cations and anionic groups.

It is noteworthy that the asymptotic decay of these reorientational correlation functions can be approximated by a biexponential decay function with the form of $C(t) = c_0 + c_1 e^{-t/\tau_1} + c_2 e^{-t/\tau_2}$.[54,57,58] The accessible fitting parameters τ_1 and τ_2 of the imidazolium ring planes in varied RTIL/water mixtures are provided in tables of the supplementary material. The slowest component time constants can be compared to the experimental values given in Table I. The fast decay mode corresponds to a free swing of the imidazolium ring planes in local ionic environments initiated by preferential hydrogen bonding interactions, and the corresponding time scale is tens of picoseconds. The continuous and intermittent hydrogen bonding interactions between the imidazolium cations, anionic groups, and water molecules lead to the constrained stretching in-and-out vibrational motion of hydrogen bonding sites.[54,57] The slow decay component is attributed to a large angular out-of-plane wagging motion of anionic groups and water molecules around the imidazolium ring planes, which results in an overall randomization of imidazolium ring planes in RTIL/water mixtures.[54,57] The time scale of the slow reorientational component is hundreds of picoseconds, which is approximately ten times slower than that for the fast relaxation mode for the same imidazolium ring planes. These two magnitudes of correlation times suggest that the overall reorientational dynamics of the imidazolium ring planes are heterogeneous depending on the delicate intermolecular interactions between constituent ions and water molecules in RTIL/water mixtures.

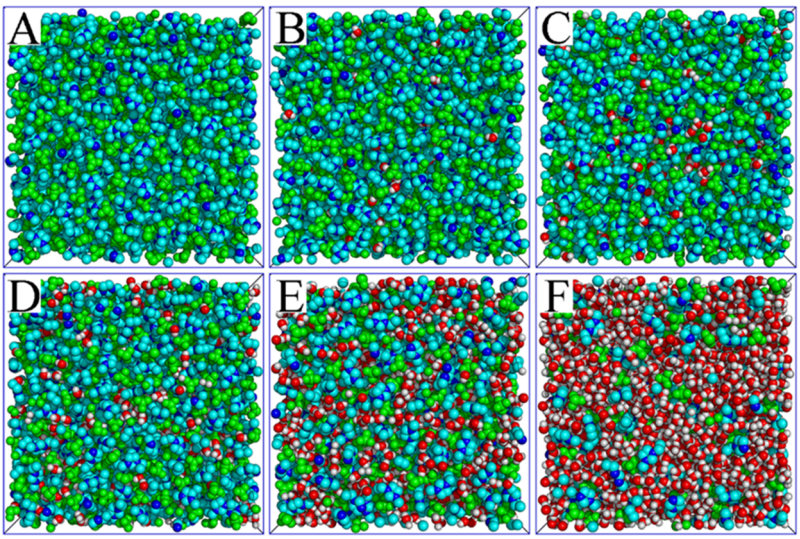

FIG. 11. Representative liquid morphologies of $EmimBF_4$ RTIL/water mixtures with varied ratios of ion pairs:water: (a) dry RTIL, (b) 8:1, (c) 2:1, (d) 1:1, (e) 1:4, and (f) 1:16. The N and C atoms in $Emim^+$ cations are represented by blue and cyan spheres, respectively. The H atoms in the $Emim^+$ cations are not shown for clarity. The BF_4^- anions are represented by green beads. The H and O atoms in water molecules are represented by light gray and red spheres, respectively.

In comparison with experimental values of τ determined from the OHD-OKE measurements listed in Table I, we can see that these computational reorientational dynamics are similar but somewhat slower than the corresponding experimental data. For the highest water concentration, the simulation and experimental data are close, but the difference increases as the water concentration decreases. For the neat $EmimBF_4$ RTIL sample, where the simulations produce the correct structure factor, the simulated orientation relaxation time is ~3 too slow. It is noteworthy that simulations producing dynamical and transport properties of RTIL/water mixtures that are too slow have been reported previously.[18,21] In the current work, we mainly focus on thermodynamics (liquid densities, as shown in Fig. 8) and microstructural description (X-ray scattering structure factors, as shown in Fig. 3) of RTIL/water mixtures from the atomistic simulations.

The reasonably good agreement between the simulations and the orientational relaxation data means that the simulations capture the rotational dynamics of imidazolium ring planes in various RTIL/water mixtures. The microstructural and dynamical characterizations of these RTIL/water mixtures promote our understanding of OHD-OKE measurements and the experimental tendencies shown in DSE plots. The NTf_2^- based RTIL/water mixtures cannot restructure as more water molecules are added because these water molecules cannot overcome the strong cation-anion interactions. This is in contrast to the BF_4-based RTIL/water mixtures where water molecules are able to infiltrate the ionic structures and induce restructuring of the local ionic environments. These microstructure differences are reflected dynamically as two distinct hydrodynamic DSE regimes.

The $EhimNTf_2$ and $EhimBF_4$ RTIL/water mixtures exhibit different DSE behavior beyond the number of linear DSE regimes depending on hydrophilicity. A distinct jump is observed in the DSE plot at 1:1 ion pairs:water in the $EhimNTf_2$ RTIL/water mixture. Atomistic simulations and FT-IR spectroscopy attributed this observation to the formation of water clusters affecting the hydrogen bonding interactions of the N–H groups in $Ehim^+$ cations with specific atoms in NTf_2^- anions. This jump is not present in the DSE plot for $EhimBF_4$. This may be attributed to the fact that water is not limited to cavities in these RTIL/water mixtures because of the smaller anionic size of BF_4^- than that of NTf_2^-.

E. Comparison of imidazolium-based BF_4^- ionic liquids as a function of cationic chain length

Another method of tuning hydrophilicity is increasing the alkyl chain length on the imidazolium cation. Previously, OHD-OKE data was taken on $BmimBF_4$ at 12 water concentrations and $HmimBF_4$ at six water concentrations.[12] These experimental results can be compared to the $EmimBF_4$ data that were discussed in Subsections III B–III D. Both $EmimBF_4$ and $BmimBF_4$ are infinitely miscible with water, while $HmimBF_4$ water saturates at 1:3 ion pairs:water. Molecular dynamics simulations have shown that there are no connected nonpolar domains in Emim-based RTILs. In Bmim-based RTILs, nonpolar regions are present but not extensive, and in $Hmim^+$ RTIL matrices, the connected nonpolar domains are ubiquitous.[59] The DSE plots of three sets of RTIL/water mixtures are given in Fig. 12. Panels (b) and (c) were reported previously[12] but panel (b) is now analyzed showing two hydrodynamic regions instead of one. In the initial report, a single line was forced through the data, which resulted in significant deviations of the data from the line. The new fit presented here reduced the χ^2 value by a factor of two when compared to the fit reported previously.

The DSE plot for the $EmimBF_4$ RTIL/water mixtures is given in Fig. 12(a). As described previously in this work, $EmimBF_4$ RTIL/water mixtures have two hydrodynamic regimes: drier than 1:2 ion pairs:water and wetter than 1:4 ion pairs:water with a crossover region. $EmimBF_4$ can restructure local ionic environments to accommodate more water without paying a substantial penalty for disturbing preferential ionic structures between polar moieties of the constituent ions. Otherwise, $EmimBF_4$ would water saturate at approximately 1:2

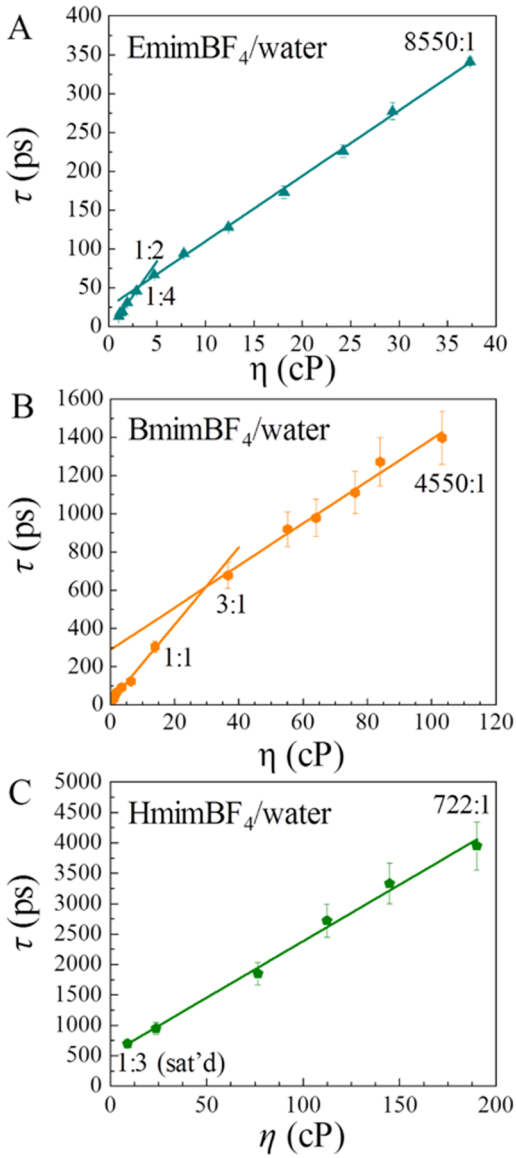

FIG. 12. The Debye Stokes Einstein plots for (a) $EmimBF_4$, (b) $BmimBF_4$, and (c) $HmimBF_4$. $EmimBF_4$ and $BmimBF_4$ are both hydrophilic and show evidence of two hydrodynamic regions, while $HmimBF_4$ is hydrophobic and is linear at all accessible water concentrations.

ion pairs:water. Instead, the microstructure of the RTIL fundamentally changes as the ions reposition themselves to allow more water into the system.

Figure 12(c) shows the DSE plot for $HmimBF_4$ RTIL/water mixtures. The saturation of $HmimBF_4$ is in contrast to that for $EmimBF_4$, which has no extended nonpolar domains and is infinitely miscible with water. The DSE plot for $HmimBF_4$ RTIL/water mixtures is linear which shows that $HmimBF_4$ RTIL/water mixtures do not fundamentally change their liquid microstructure as the water concentration increases. The $HmimBF_4$ RTIL/water samples are hydrodynamic, which matches the observations of the other hydrophobic samples. This is likely due to preferential dispersion interactions among alkyl units in the imidazolium cations, making it unfavorable for ionic moieties to change local microstructures to accommodate more water molecules. Instead of disturbing the extended nonpolar network, $HmimBF_4$ saturates with water.

The DSE plot for $BmimBF_4$ RTIL/water mixtures is shown in Fig. 12(b). $BmimBF_4$ is the intermediate case in which the connected nonpolar domains are present to a limited extent. Similar to the DSE plot for $EmimBF_4$ RTIL/water mixtures, there are two linear regimes: a moderately sloped low water content regime and a steeply sloped high water content regime. However, the transition point in the $BmimBF_4$ RTIL/water mixtures is between 3:1 and 1:1 ion pairs:water, a lower water concentration than that observed in $EmimBF_4$ RTIL/water mixtures. The $Bmim^+$ cations are able to restructure local ionic structures to allow the addition of more water, giving rise to the two linear regimes because the nonpolar domains are less extensive than those in the $HmimBF_4$ RTIL/water mixtures. However, although the nonpolar domains in $BmimBF_4$ are relatively minor in extent, they are associated with restructuring at a lower water concentration than that in $EmimBF_4$ RTIL/water mixtures.

The behaviors of the three different chain length RTILs can be considered in terms of liquid density of the RTIL/water mixtures, as shown in Fig. 13. The liquid densities were interpolated from the literature.[55] The density of $HmimBF_4$ remains almost constant, decreasing just 2.7% between the dry and water saturated samples. The small change in liquid density further supports the idea that the microstructure of $HmimBF_4$ does not change significantly with the gradual addition of water. This ionic liquid phase separates rather than restructuring. As mentioned previously, the liquid density of $EmimBF_4$ only decreases by 4.9% between the dry sample and the 1:2 sample [the last sample of the first linear regime in Fig. 12(a)]. After this concentration, the liquid density begins decreasing quickly as it approaches the density of water. The intermediate case of $BmimBF_4$ RTIL/water mixtures is slightly more complicated. The densities of the $BmimBF_4$/water mixtures are fairly constant until 1:3 ion pairs:water. At this point, the density begins to drop quickly. This suggests that the water accommodating structural changes of $BmimBF_4$ is inhibited by favorable van der Waals interactions between butyl chains in $Bmim^+$ cations that are not present in $EmimBF_4$ and $EhimBF_4$ RTIL/water mixtures. The initial restructuring of the limited nonpolar regions in $BmimBF_4$ must involve subtle changes that do not affect the density. Something else to note is that at high water concentration, the $EmimBF_4$ and $BmimBF_4$ RTIL/water mixtures have the same liquid densities, which suggests that at high water concentrations, the alkyl chains in the $Bmim^+$ cations are no longer playing a significant role in accommodating water into the RTIL medium.

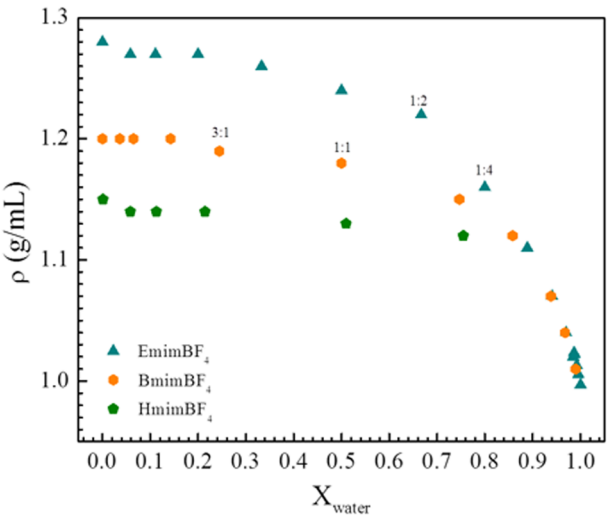

FIG. 13. Liquid densities of $EmimBF_4$ (blue), $BmimBF_4$ (orange), and $HmimBF_4$ (green) as a function of water content.

Anomalous behavior for $BmimBF_4$ RTIL/water mixtures has been observed in atomistic simulations, fluorescence experiments, and 2D-IR experiments. Atomistic simulations conducted by Voth and co-workers have shown that there is a breakdown of the limited nonpolar domains in $BmimBF_4$ RTIL/water mixtures around 1:3 ion pairs:water, consistent with our observations. The nonpolar domains do not break down in longer chained BF_4^- ionic liquids.[60] In fluorescence anisotropy experiments, the experimental friction of $HmimBF_4$ and longer-chained cations with BF_4^- increased as water content increased up to the saturation point.[16] For $BmimBF_4$ RTIL/water mixtures, the friction initially increased as water was added; however, between the 1:1 and 1:3 samples, the friction drops and continues to decrease as more water is added. This was attributed to cation reorientation not being inhibited by large nonpolar domains. Finally, 2D-IR experiments on $BmimBF_4$ suggested a unique cooperation between the polar region and nonpolar domains as the ionic liquid restructures. This is absent in BF_4^-based RTILs with longer alkyl chains in imidazolium cations.[61]

IV. CONCLUDING REMARKS

The influence of ionic liquid hydrophilicity on the dynamics and microstructures of ionic liquid/water mixtures was studied using Optical Heterodyne-Detected Optical Kerr Effect (OHD-OKE) spectroscopy and atomistic molecular dynamics simulations. Hydrophilicity was tuned via anion selection, cation chain length, and the addition of strong hydrogen bonding groups. Debye Stokes Einstein (DSE) plots from the OHD-OKE data demonstrated a fundamental difference

between hydrophilic (infinitely water miscible) ionic liquids and hydrophobic (water saturating) ionic liquids. Hydrophobic ionic liquids exhibited DSE behavior at all water concentrations indicating that not taking up water is more favorable than restructuring to allow for the addition of more water. This is in contrast to hydrophilic ionic liquids, where two distinct hydrodynamic regions are observed in the DSE plot. At low water concentrations, the DSE plot is linear with a small slope. At high water concentrations, a new linear regime is entered with a much steeper slope. This suggests that the microscopic ionic structures in RTIL/water mixtures fundamentally change to allow more water to be taken up. When it is unfavorable for the microstructure to change, the ionic liquid becomes saturated and phase separation occurs. Saturation is observed in all NTf_2^- samples, while in cations with short alkyl chains ($Emim^+$ and $Bmim^+$) paired with BF_4^-, saturation does not occur. However, when the alkyl chain becomes long, e.g., $HmimBF_4$, the hydrophobic alkyl chain causes saturation to occur, as seen in all NTf_2-based samples. In protic ionic liquids, e.g., $Ehim^+$, saturation occurs when the anion is NTf_2^- but not when BF_4^- is the anion. Atomistic simulations demonstrated that local ionic structures experience distinct changes in the hydrophilic and hydrophobic RTIL/water mixtures because of the delicate balance of intermolecular interactions among imidazolium cations, hydrophilic/hydrophobic anions, and water molecules.

Previously, it has been established that hydrophilicity is highly structure dependent and is particularly sensitive to anion selection.[11] Studies on the influence of anion selection have shown that hydrophobicity often occurs in RTILs with perfluorinated groups suggesting the role of hydrogen bonding in hydrophilicity.[62] In the current work, the relationship between intermolecular interactions and hydrophilicity is further explored. The results presented here demonstrate that multiple ionic liquids have stronger interactions that make restructuring unfavorable, resulting in water saturation and hydrophobic behavior. In the case of $EmimNTf_2$ and $EhimNTf_2$, this is due to strong cation-anion interactions that are unfavorable to break, as shown by the atomistic simulations. In the case of $HmimBF_4$, preferential dispersion interactions between the alkyl chains that comprise the extended network of nonpolar domains limit reorganization to accommodate additional water molecules.

This behavior is in contrast to hydrophilic samples which have weaker interactions that allow constituent ions to structurally rearrange. As shown in atomistic simulations, $EmimBF_4$ and $EhimBF_4$ have weaker cation-anion interactions than their NTf_2^- analogs. Thus, it is favorable to alter these interactions to accommodate more water. $BmimBF_4$ has more limited nonpolar domains than $HmimBF_4$, which results in weaker alkyl chain interactions. Thus, it is still favorable to break these interactions. The experimental and computational results presented here have provided a broader understanding of hydrophilicity in ionic liquids. OHD-OKE, density measurements, and atomistic simulations demonstrated that the strength of intermolecular interactions and the ability for constituent ions to restructure are the key driving forces for hydrophilicity in ionic liquids.

SUPPLEMENTAL MATERIAL

See supplementary material for the synthesis and characterization of $EhimBF_4$, additional OHD-OKE fits, representative radial distribution functions, and the rotational dynamics of imidazolium ring planes in varied RTIL/water mixtures.

ACKNOWLEDGMENTS

We thank Joseph E. Thomaz for synthesis assistance. H.E.B. and M.D.F. acknowledge financial support from the Division of Chemistry, Directorate of Mathematical and Physical Sciences, National Science Foundation (NSF) (No. CHE-1461477). Y.-L. Wang gratefully acknowledges the financial support from Knut and Alice Wallenberg Foundation (No. KAW 2015.0417). Atomistic molecular dynamics simulations were performed using computational resources provided by Stanford University. Part of this work was performed at the Stanford Nano Shared Facilities (SNSF), supported by the National Science Foundation under Award No. ECCS-1542152. NMR spectra were collected at the Stanford University Department of Chemistry NMR facility.

[1] E. W. Castner, C. J. Margulis, M. Maroncelli, and J. F. Wishart, "Ionic liquids: Structure and photochemical reactions," Annu. Rev. Phys. Chem. **62**, 85–105 (2011).
[2] R. Hayes, G. G. Warr, and R. Atkin, "Structure and nanostructure in ionic liquids," Chem. Rev. **115**, 6357–6426 (2015).
[3] M. Armand, F. Endres, D. R. MacFarlane, H. Ohno, and B. Scrosati, "Ionic-liquid materials for the electrochemical challenges of the future," Nat. Mater. **8**, 621–629 (2009).
[4] M.-C. Lin, M. Gong, B. Lu, Y. Wu, D.-Y. Wang, M. Guan, M. Angell, C. Chen, J. Yang, B.-J. Hwang, and H. Dai, "An ultrafast rechargeable aluminium-ion battery," Nature **520**, 324–328 (2015).
[5] D. R. MacFarlane, N. Tachikawa, M. Forsyth, J. M. Pringle, P. C. Howlett, G. D. Elliott, J. H. Davis, M. Watanabe, P. Simon, and C. A. Angell, "Energy applications of ionic liquids," Energy Environ. Sci. **7**, 232–250 (2014).
[6] S. M. Zakeeruddin and M. Graetzel, "Solvent-free ionic liquid electrolytes for mesoscopic dye-sensitized solar cells," Adv. Funct. Mater. **19**, 2187–2202 (2009).
[7] X. Zhang, X. Zhang, H. Dong, Z. Zhao, S. Zhang, and Y. Huang, "Carbon capture with ionic liquids: Overview and progress," Energy Environ. Sci. **5**, 6668–6681 (2012).
[8] T. Welton, "Room-temperature ionic liquids. Solvents for synthesis and catalysis," Chem. Rev. **99**, 2071–2084 (1999).
[9] A. Riisagera, R. Fehrmanna, M. Haumannb, and P. Wasserscheidb, "Supported ionic liquids: Versatile reaction and separation media," Top. Catal. **40**, 91–102 (2006).
[10] J. A. Widegren, A. Laesecke, and J. W. Magee, "The effect of dissolved water on the viscosities of hydrophobic room-temperature ionic liquids," Chem. Commun. **2005**, 1610–1612.
[11] J. G. Huddleston, A. E. Visser, W. M. Reichert, H. D. Willauer, G. A. Broker, and R. D. Rogers, "Characterization and comparison of hydrophilic and hydrophobic room temperature ionic liquids incorporating the imidazolium cation," Green Chem. **3**, 156–164 (2001).
[12] A. L. Sturlaugson, K. S. Fruchey, and M. D. Fayer, "Orientational dynamics of room temperature ionic liquid/water mixtures: Evidence for water-induced structure and anisotropic cation solvation," J. Phys. Chem. B **116**, 1777–1787 (2012).
[13] S. Rivera-Rubero and S. Baldelli, "Influence of water on the surface of hydrophilic and hydrophobic room-temperature ionic liquids," J. Am. Chem. Soc. **126**, 11788–11789 (2004).
[14] H. E. Bailey, Y.-L. Wang, and M. D. Fayer, "Impact of hydrogen bonding on the dynamics and structure of protic ionic liquid/water binary mixtures," J. Phys. Chem. B **121**, 8564–8576 (2017).
[15] A. L. Sturlaugson, A. Y. Arima, H. E. Bailey, and M. D. Fayer, "Orientational dynamics in a lyotropic room temperature ionic liquid," J. Phys. Chem. B **117**, 14775–14784 (2013).

[16]J. E. Thomaz, C. M. Lawler, and M. D. Fayer, "The influence of water on the alkyl region structure in variable chain length imidazolium-based ionic liquid/water mixtures," J. Phys. Chem. B **120**, 10350–10357 (2016).
[17]N. Yaghini, V. Gómez-González, L. M. Varela, and A. Martinelli, "Structural origin of proton mobility in a protic ionic liquid/imidazole mixture: Insights from computational and experimental results," Phys. Chem. Chem. Phys. **18**, 23195–23206 (2016).
[18]N. Yaghini, L. Nordstierna, and A. Martinelli, "Effect of water on the transport properties of protic and aprotic imidazolium ionic liquids—An analysis of self-diffusivity, conductivity, and proton exchange mechanism," Phys. Chem. Chem. Phys. **16**, 9266–9275 (2014).
[19]G. Driver, Y. Huang, A. Laaksonen, T. Sparrman, Y.-L. Wang, and P.-O. Westlund, "Correlated/non-correlated ion dynamics of charge-neutral ion couples: The origin of ionicity in ionic liquids," Phys. Chem. Chem. Phys. **19**, 4975–4988 (2017).
[20]A. Martinelli, "Conformational changes and phase behaviour in the protic ionic liquid 1-ethylimidazolium bis (trifluoromethylsulfonyl) imide in the bulk and nano-confined State," Eur. J. Inorg. Chem. **2015**, 1300–1308.
[21]A. Martinelli, M. Maréchal, Å. Östlund, and J. Cambedouzou, "Insights into the interplay between molecular structure and diffusional motion in 1-alkyl-3-methylimidazolium ionic liquids: A combined PFG NMR and x-ray scattering study," Phys. Chem. Chem. Phys. **15**, 5510–5517 (2013).
[22]A. Mele, C. D. Tran, and S. H. De Paoli Lacerda, "The structure of a room-temperature ionic liquid with and without trace amounts of water: The role of C–H$\cdots$O and C–H$\cdots$F interactions in 1-n-butyl-3-methylimidazolium tetrafluoroborate," Angew. Chem., Int. Ed. **42**, 4364–4366 (2003).
[23]M. Krüger, E. Bründermann, S. Funkner, H. Weingärtner, and M. Havenith, "Communications: Polarity fluctuations of the protic ionic liquid ethylammonium nitrate in the terahertz regime," J. Chem. Phys. **132**, 101101 (2010).
[24]B. Bhargava, Y. Yasaka, and M. L. Klein, "Computational studies of room temperature ionic liquid–water mixtures," Chem. Commun. **47**, 6228–6241 (2011).
[25]T. Méndez-Morales, J. Carrete, O. Cabeza, L. J. Gallego, and L. M. Varela, "Molecular dynamics simulation of the structure and dynamics of water–1-alkyl-3-methylimidazolium ionic liquid mixtures," J. Phys. Chem. B **115**, 6995–7008 (2011).
[26]Y.-L. Wang, M. R. Shimpi, S. Sarman, O. N. Antzutkin, S. Glavatskih, L. Kloo, and A. Laaksonen, "Atomistic insight into tetraalkylphosphonium bis(oxalato)borate ionic liquid/water mixtures. II. Volumetric and dynamic properties," J. Phys. Chem. B **120**, 7446–7455 (2016).
[27]Y.-L. Wang, S. Sarman, L. Kloo, O. N. Antzutkin, S. Glavatskih, and A. Laaksonen, "Solvation structures of water in trihexyltetradecylphosphonium-orthoborate ionic liquids," J. Chem. Phys. **145**, 064507 (2016).
[28]Y.-L. Wang, S. Sarman, S. Glavatskih, O. N. Antzutkin, M. W. Rutland, and A. Laaksonen, "Atomistic insight into tetraalkylphosphonium-bis (oxalato) borate ionic liquid/water mixtures. I. Local microscopic structure," J. Phys. Chem. B **119**, 5251–5264 (2015).
[29]T. Wu, S. Su, S. Gung, M. Lin, Y. Lin, W. Ou-Yang, I. Sun, and C. Lai, "Synthesis and characterization of protic ionic liquids containing cyclic amine cations and tetrafluoroborate anion," J. Iran. Chem. Soc. **8**, 149–165 (2011).
[30]G. L. Burrell, I. M. Burgar, F. Separovic, and N. F. Dunlop, "Preparation of protic ionic liquids with minimal water content and ^{15}N NMR study of proton transfer," Phys. Chem. Chem. Phys. **12**, 1571–1577 (2010).
[31]A. K. Burrell, R. E. D. Sesto, S. N. Baker, T. M. McCleskey, and G. A. Baker, "The large scale synthesis of pure imidazolium and pyrrolidinium ionic liquids," Green Chem. **9**, 449–454 (2007).
[32]A. Tamimi, H. E. Bailey, and M. D. Fayer, "Alkyl chain length dependence of the dynamics and structure in the ionic regions of room-temperature ionic liquids," J. Phys. Chem. B **120**, 7488–7501 (2016).
[33]E. Rilo, J. Vila, J. Pico, S. Garciva-Garabal, L. Segade, L. M. Varela, and O. Cabeza, "Electrical conductivity and viscosity of aqueous binary mixtures of 1-alkyl-3-methyl imidazolium tetrafluoroborate at four temperatures," J. Chem. Eng. Data **55**, 639–644 (2009).
[34]S. Kinoshita, Y. Sakai, J. Miyazaki, and J. Watanabe, "Fundamental aspects of light scattering and optical Kerr effect spectroscopy," Eur. Phys. J.: Spec. Top. **209**, 1–100 (2012).
[35]N. A. Smith and S. R. Meech, "Optically-heterodyne-detected optical Kerr effect (OHD-OKE): Applications in condensed phase dynamics," Int. Rev. Phys. Chem. **21**, 75–100 (2002).
[36]J. Li, H. Cang, H. C. Anderson, and M. D. Fayer, "A mode coupling theory description of the short and long-time dynamics of nematogens in the isotropic phase," J. Chem. Phys. **124**, 014902 (2006).
[37]W. Götze and L. Sjögren, "The mode coupling theory of structural relaxations," Transp. Theory Stat. Phys. **24**, 801–853 (1995).
[38]M. J. Abraham, T. Murtola, R. Schulz, S. Páll, J. C. Smith, B. Hess, and E. Lindahl, "GROMACS: High performance molecular simulations through multi-level parallelism from laptops to supercomputers," SoftwareX **1**, 19–25 (2015).
[39]F. W. Deeg, J. J. Stankus, S. R. Greenfield, V. J. Newell, and M. D. Fayer, "Anisotropic reorientational relaxation of biphenyl: Transient grating optical Kerr effect measurements," J. Chem. Phys. **90**, 6893 (1989).
[40]S. Ruhman, L. R. Williams, A. G. Joly, B. Kohler, and K. A. Nelson, "Nonrelaxational inertial motion in CS_2 liquid observed by time-resolved impulsive stimulated scattering," J. Phys. Chem. **91**, 2237–2240 (1987).
[41]S. Palese, L. Schilling, R. D. Miller, P. R. Staver, and W. T. Lotshaw, "Femtosecond optical Kerr effect studies of water," J. Phys. Chem. **98**, 6308–6316 (1994).
[42]A. Taschin, P. Bartolini, R. Eramo, R. Righini, and R. Torre, "Optical Kerr effect of liquid and supercooled water: The experimental and data analysis perspective," J. Chem. Phys. **141**, 084507 (2014).
[43]R. Torre, P. Bartolini, and R. Righini, "Structural relaxation in supercooled water by time-resolved spectroscopy," Nature **428**, 296–299 (2004).
[44]G. Giraud, C. M. Gordon, I. R. Dunkin, and K. Wynne, "The effects of anion and cation substitution on the ultrafast solvent dynamics of ionic liquids: A time-resolved optical Kerr-effect spectroscopic study," J. Chem. Phys. **119**, 464–477 (2003).
[45]A. L. Sturlaugson, *Orientational Dynamics in Water/Cosolvent Mixtures* (Stanford University, 2013).
[46]S. A. Allison, "Low Reynolds number transport properties of axisymmetric particles employing stick and slip boundary conditions," Macromolecules **32**, 5304–5312 (1999).
[47]C.-M. Hu and R. Zwanzig, "Rotational friction coefficients for spheroids with the slipping boundary condition," J. Chem. Phys. **60**, 4354–4357 (1974).
[48]M. M. Tirado and J. G. de la Torre, "Rotational dynamics of rigid, symmetric top macromolecules. Application to circular cylinders," J. Chem. Phys. **73**, 1986–1993 (1980).
[49]T. Takamuku, Y. Kyoshoin, T. Shimomura, S. Kittaka, and T. Yamaguchi, "Effect of water on structure of hydrophilic imidazolium-based ionic liquid," J. Phys. Chem. B **113**, 10817–10824 (2009).
[50]Y.-L. Wang, A. Laaksonen, and M. D. Fayer, "Hydrogen bonding versus π–π stacking interactions in imidazolium–oxalatoborate ionic liquid," J. Phys. Chem. B **121**, 7173–7179 (2017).
[51]K. Fumino, A. Wulf, and R. Ludwig, "Strong, localized, and directional hydrogen bonds fluidize ionic liquids," Angew. Chem., Int. Ed. **47**, 8731–8734 (2008).
[52]H. Weber, O. Hollóczki, A. S. Pensado, and B. Kirchner, "Side chain fluorination and anion effect on the structure of 1-butyl-3-methylimidazolium ionic liquids," J. Chem. Phys. **139**, 084502 (2013).
[53]B. Qiao, C. Krekeler, R. Berger, L. Delle Site, and C. Holm, "Effect of anions on static orientational correlations, hydrogen bonds, and dynamics in ionic liquids: A simulational study," J. Phys. Chem. B **112**, 1743–1751 (2008).
[54]Y.-L. Wang, "Competitive microstructures vs. cooperative dynamics of hydrogen bonding and π type stacking interactions in imidazolium bis (oxalato) borate ionic liquids," J. Phys. Chem. B **122**, 6570–6585 (2018).
[55]E. Rilo, J. Pico, S. García-Garabal, L. Varela, and O. Cabeza, "Density and surface tension in binary mixtures of C_nMIM-BF_4 ionic liquids with water and ethanol," Fluid Phase Equilib. **285**, 83–89 (2009).
[56]S. Cerimovic, R. Beigelbeck, H. Antlinger, J. Schalko, B. Jakoby, and F. Keplinger, "Viscosity and density measurements of glycerol-water mixtures utilizing a novel resonant MEMS sensor," in Smart Sensors, Actuators, and MEMS V, 2011, Proc. SPIE **8066**, 80662E (2011).
[57]R. P. Matthews, T. Welton, and P. A. Hunt, "Hydrogen bonding and π–π interactions in imidazolium-chloride ionic liquid clusters," Phys. Chem. Chem. Phys. **17**, 14437–14453 (2015).
[58]Y.-L. Wang, Y.-L. Zhu, Z.-Y. Lu, and A. Laaksonen, "Electrostatic interactions in soft particle systems: Mesoscale simulations of ionic liquids," Soft Matter **14**, 4252–4267 (2018).

[59]J. N. A. Canongia Lopes and A. A. H. Pádua, "Nanostructural organization in ionic liquids," J. Phys. Chem. B **110**, 3330–3335 (2006).
[60]S. Feng and G. A. Voth, "Molecular dynamics simulations of imidazolium-based ionic liquid/water mixtures: Alkyl side chain length and anion effects," Fluid Phase Equilib. **294**, 148–156 (2010).
[61]C. H. Giammanco, P. L. Kramer, D. B. Wong, and M. D. Fayer, "Water dynamics in 1-alkyl-3-methylimidazolium tetrafluoroborate ionic liquids," J. Phys. Chem. B **120**, 11523–11538 (2016).
[62]J. M. Pringle, J. Golding, K. Baranyai, C. M. Forsyth, G. B. Deacon, J. L. Scott, and D. R. MacFarlane, "The effect of anion fluorination in ionic liquids—physical properties of a range of bis (methanesulfonyl) amide salts," New J. Chem. **27**, 1504–1510 (2003).
[63]J. E. Thomaz, H. E. Bailey, and M. D. Fayer, "The influence of mesoscopic confinement on the dynamics of imidazolium-based room temperature ionic liquids in polyether sulfone membranes," J. Chem. Phys. **147**, 194502 (2017).